Experimental Characterization of Emulsion Formation and Coalescence by Nuclear Magnetic Resonance Restricted Diffusion Techniques

H.-Y. Lee[a,1], M.J. McCarthy[b,c], and S.R. Dungan[a,b,*]

Departments of [a]Chemical Engineering and Materials Science, [b]Food Science and Technology, and [c]Biological and Agricultural Engineering, University of California, Davis, California 95616

ABSTRACT: Nuclear magnetic resonance (NMR) is explored as a technique for noninvasively monitoring emulsion droplet formation and destabilization. The method makes use of the fact that the diffusion of oil molecules within oil-in-water emulsion droplets results in attenuation of a coherent magnetic signal that emanates from those molecules. If oil diffusion is limited by the size of the droplet, the shape of a plot of attenuation over time is directly affected by the droplet radius. We use this approach to determine noninvasively the effect of surfactant type, surfactant concentration, pH, and ionic strength on droplet sizes within a 40 wt% octane and water emulsion, stabilized by Tween 20 or β-lactoglobulin (β-Lg). We find that addition of the low-molecular-weight Tween 20 forms finer emulsion droplets than does addition of the protein, and that the Tween 20 emulsion is sensitive to surfactant concentration below a threshold "saturation" concentration. The droplet sizes in β-Lg-containing emulsions increase as pH increases above the isoelectric point and as ionic strength increases. The fact that the NMR technique does not mistake clusters of droplets for single large droplets makes the analysis of these effects unambiguous. We further extend the use of NMR diffusion techniques to monitor the effect of surfactant type, surfactant concentration, and convection on the rate of droplet coalescence. The ability of NMR methods to distinguish between large single droplets and droplet clusters makes it well-suited to monitor coalescence processes independently from flocculation.

JAOCS 75, 463–475 (1998).

KEY WORDS: Coalescence, droplet sizes, emulsification, emulsion formation, emulsions, β-lactoglobulin, NMR restricted diffusion, Tween 20.

An emulsion is a mixture of two immiscible liquids and contains a dispersed phase, which consists of fine droplets with diameters greater than 0.1 μm, as well as a continuous phase in which the droplets are suspended. Such systems are thermodynamically unstable and will separate into two distinct phases after a sufficient period of time. The addition of emulsifiers—e.g., synthetic surfactants or proteins—is often necessary to help in the formation and stabilization of the drops, thereby increasing the lifetime of the emulsion through their effects on the interfacial tension and interparticle interactions. Because many foods, cosmetics, and pharmaceutical formulations are made up of emulsions (e.g., milk, mayonnaise, margarine, salad dressing, and skin creams), a better understanding is needed of the relationship between emulsion properties and the quality and stability of such products.

The formation of an emulsion with finely dispersed droplets requires that added emulsifiers rapidly adsorb at newly created oil/water interfaces, where they lower the interfacial tension and prevent recoalescence. Once formed, the emulsion can phase-separate as a result of three dominant breakdown processes, known as creaming, flocculation, and coalescence. Creaming is the separation of an emulsion into a concentrated and a dilute fraction due to a density difference between the two liquid phases. In flocculation, two or more droplets cluster together with no change in droplet sizes. Coalescence causes two or more droplets to merge together to form a single larger droplet, leading to an irreversible change in droplet size distribution. Because flocculation and coalescence directly affect the structure of the emulsion, change in droplet (or cluster) size with time is a basic measure of the extent of coalescence or flocculation.

Studies have been conducted to characterize the stability of emulsions against coalescence by monitoring the evolution of droplet size distributions over time (1–10). Different techniques have been employed to measure emulsion droplet sizes, such as particle size analysis in a Coulter counter (3,4), turbidity measurements (5,6,9), light-scattering methods (2,7,8), and electron microscopy (10). However, most of these methods suffer from a common drawback in that their sampling techniques are invasive or destructive to the sample (e.g., dilution, freezing). Hence, the original structure of the emulsion can be destroyed or changed by the measuring technique itself. In addition, the inability to distinguish aggregates from large single particles in an emulsion can result in sizing inaccuracy, and hence misinterpretation of results.

Nuclear magnetic resonance (NMR) was first utilized by Packer and Rees (11) to provide a measure of the droplet size distribution of an emulsion in a noninvasive manner. This

[1]Present address: Alza Corporation, 700 Eubanks Dr., Vacaville, CA 95688.
*To whom correspondence should be addressed.
E-mail: srdungan@ucdavis.edu.

method is based on the measurement by NMR techniques of the extent of molecular diffusion within a sample. Because the distance that oil molecules can diffuse within emulsion droplets is limited by the size of the droplets, NMR can be used to quantify the size distribution of droplets within an emulsion. Since the introduction of this method by Packer and Rees, there have been efforts to apply this method to the structural characterization of emulsions (12–15).

In the present paper, we discuss studies in which this NMR diffusion technique is utilized to distinguish between emulsion types, i.e., an oil-in-water emulsion (o/w) and a water-in-oil (w/o) emulsion, and to provide direct measurement of the droplet size distribution. Also, the effect of emulsifying variables, such as emulsifier concentration, the nature of the emulsifier, salt concentration and pH, on the emulsion properties is examined. By monitoring droplet size distributions over time, we extend this technique to the determination of droplet coalescence processes. NMR methods have a unique applicability to the study of coalescence: because the technique relies on molecular diffusion within the droplet, it detects size increases in the droplets themselves, rather than clustering of smaller droplets. Thus, this technique can noninvasively distinguish coalescence from flocculation. In the study described here, the effect of emulsifier concentration and induced convection on the coalescence stability is investigated through NMR techniques.

THEORY

NMR measurement of the self-diffusion coefficient. In an NMR experiment, nuclei that possess a nuclear magnetic moment precess about an external field with a frequency ω_o given by the Larmor relationship $\omega_o = \gamma B_o$ (16). Here, γ is the gyromagnetic ratio ($\gamma = 42.576$ MHz/T for ^{1}H), and B_o is the external magnetic field applied to the system. If, in addition to the constant magnetic field, one adds a magnetic field gradient that varies linearly in space with slope g, the frequency of the precessing nuclei will also vary linearly in space. By further applying a radio frequency pulse of frequency ω_o to the system, the nuclei absorb radiation energy and are displaced from equilibrium. In the absence of a magnetic field gradient, the process by which the excited nuclei return to the equilibrium state is characterized by a first-order exponential decay, with time constants T_1 (spin-lattice relaxation) and T_2 (spin-spin relaxation). However, in the presence of such a gradient, if the spin makes a random jump owing to Brownian motion to a new position during the measurement, it will move to a region with a different magnetic field strength. The result is that the diffusive motion causes an irreversible loss in phase coherence, which leads to an additional decay of the signal intensity. The extent of this decay is related to the extent of diffusive motion.

The pulsed field gradient (PFG) NMR technique, as developed by Stejskal and Tanner (17), has been widely applied for the detection of the effect of diffusion that occurs during the time interval Δ between two gradient pulses. In this method, the NMR attenuation R is defined as the ratio of signal intensities M with and without the presence of a gradient field, recognizing that the measurement is insensitive to diffusional processes in the absence of the gradient field. The self-diffusion coefficient D of a pure liquid can be determined by the measurement of this attenuation, from the relation (18) (Equation 1):

$$R = \frac{M(g)}{M(\mathrm{O})} = \exp[-D\delta^2\gamma^2 g^2(\Delta - \delta/3)] \qquad [1]$$

where δ is the duration of the applied gradient field and g is again the magnitude of the applied gradient. As defined above, the NMR signal attenuation eliminates the effects of relaxation times T_1 and T_2, and therefore solely depends on the extent of molecular diffusion.

Determination of droplet size by NMR restricted diffusion measurements. In a heterogeneous system, the translational motion of diffusing molecules is strongly influenced by the sample internal structure. In a confined geometry, the maximal extent of diffusional displacement is limited by the size of the confinement. For example, the transport of water molecules within plant vascular tubes and the diffusion of oil molecules within emulsion droplets are restricted by the geometry and dimensions of the internal boundaries within those systems. The effect of this so-called restricted diffusion on PFG–NMR measurements was studied by Murday and Cotts (18). By calculating the accumulation of phase shifts during a PFG experiment, the expression for signal attenuation R for a spherical boundary of radius a is determined to be (19) (Equation 2):

$$R = \exp\left[-2\gamma^2 g^2 \sum_{m=1}^{\infty} \frac{1}{\alpha_m^2(\alpha_m^2 a^2 - 2)} \times \left\{\frac{2\delta}{\alpha_m^2 D} - \frac{2 + e^{-\alpha_m^2 D(\Delta - \delta)} - 2e^{-\alpha_m^2 D\delta} - 2e^{-\alpha_m^2 D\Delta} + e^{-\alpha_m^2 D(\Delta + \delta)}}{(\alpha_m^2 D)^2}\right\}\right]. \qquad [2]$$

Here, α_m is the mth root of the equation $J_{3/2}(\alpha_m a) = \alpha_m a J_{5/2}(\alpha_m a)$, with $J_p(x)$ the Bessel function of order p. It can be shown that, when the diffusion distance is small compared to the droplet radius, $(6D\Delta)^{1/2} << a$, Equation 2 reduces to Equation 1, and the expression for unrestricted diffusion is recovered.

For an emulsion, Packer and Rees (11) suggested that, owing to the polydispersity of droplet sizes, the experimentally observed echo attenuation is a sum of the echo contributions from individual droplets weighted by the volume of each droplet (Equation 3):

$$R_{\mathrm{obs}}(\Delta, g, \delta) = \frac{\int_0^\infty a^3 P(a) R(\Delta, g, \delta; D, a) da}{\int_0^\infty a^3 P(a) da} \qquad [3]$$

Here, $R(\Delta,g,\delta;D,a)$ is the signal attenuation given by Equa-

tion 2, and $P(a)$ is the log-normal distribution function represented by (Equation 4):

$$P(a) = \frac{1}{2a\sigma(2\pi)^{1/2}} \exp\left[-\frac{(\ln 2a - \ln 2\bar{a})^2}{2\sigma^2}\right] \quad [4]$$

The parameters $\bar{a}$ σ in Equation 4 are the mean radius and the standard deviation of the distribution, respectively. By substituting Equation 4 into Equation 3 and curve-fitting the experimental data to obtain $\bar{a}$ and σ, the droplet size distribution of emulsions can be determined. Probabilities other than a log-normal distribution also can be used in place of Equation 4.

EXPERIMENTAL PROCEDURES

Materials. The hydrocarbon oil used in our study was *n*-octane (95% pure), which we obtained from Fisher Chemical Co. (Pittsburgh, PA). Some emulsions were formed with commercial-grade polyoxyethylene sorbitan monolaurate (Tween 20), a nonionic surfactant, which was purchased from Sigma Chemical Company (St. Louis, MO). Tween 20 has a molecular weight of 1228 g/mol. The protein β-lactoglobulin (β-Lg), a major protein in milk, was also employed as an emulsifier. This protein has an isoelectric point (pI) of 5.2 and a molecular weight of 36,000 Da. β-Lg was also obtained from Sigma and used without further purification. Deuterium oxide (D_2O) with 99.9% ^2H was provided by Aldrich Chemical Company (Milwaukee, WI).

Emulsion preparation. Coarse emulsions were prepared with an Ultra-Turrax T25 high-speed blender (Janke & Kunkell, Cincinnati, OH) by mixing *n*-octane with an aqueous phase that contained 0.1 wt% β-Lg, or 0.1–3.0 wt% Tween 20 in solution. The resulting dispersion contained 40 wt% *n*-octane. These emulsions were then further homogenized in a home-built single-piston recirculating valve homogenizer. The droplet sizes were controlled by varying the number of times through the homogenizer and the duration of mixing in the blender.

NMR diffusion measurements. NMR measurements of the o/w emulsions at 18°C were performed with an Oxford Instruments 7 Tesla superconducting magnet (Eynsham, United Kingdom), a General Electric Omega spectrometer console (Fremont, CA), and Nalorac Cryogenics gradients (Martinez, CA) driven by Techron Amplifiers (Elkhart, IN). A solenoid coil with diameter of 3/8″ and total length of 5 mm was constructed and tuned to 300 MHz to measure the ^1H signal. The sample was contained in 5-mm i.d. NMR tubes, which were approximately 3 cm in length. The gradient coils were used to generate linear variations in the magnetic field across the sample. By using NMR one-dimensional imaging, the gradient strength was calibrated by measuring the size of a sphere with known diameter.

NMR pulse sequence. The proton spin-spin relaxation time T_2 of *n*-octane in an o/w emulsion sample was measured by using a Hahn spin-echo sequence (19). The observed value was less than 100 ms. This relatively short T_2 limits duration of the diffusion times Δ we can use in the spin-echo method because, if $\Delta \geq T_2$, most of the signal is lost to relaxation effects before a measurement can be made. This problem can be overcome by using the stimulated echo method, which takes advantage of the relatively long T_1 relaxation, which we measured to be 1.57 s. The pulse sequence of the stimulated echo method is shown in Figure 1. With the external magnetic field pointing in the z direction, an initial 90° pulse at time zero rotates the magnetization vector **M** onto the +y axis, after which time the spins begin to fan out and lose phase coherence owing to the spin-spin relaxation and field inhomogeneities. A second pulse applied at time τ_1 stores the memory of the current phase angles in the z-direction, where the spin-lattice (longitudinal) relaxation takes place. The third 90° pulse at time τ_2 turns **M** onto the −y axis to remove the effect of field inhomogeneities, and thereby restores the phase angles [see Callaghan (20) for a more detailed description of this procedure]. In our system, where $T_1 > T_2$, the use of a stimulated echo provides an extended range of time for diffusion measurements.

In our experiments, the gradient field strength *g* was varied from 0 to 30 G/cm. The diffusion time Δ between pulses was typically 250 ms, and the gradient pulse width δ ranged between 5 and 25 ms. The signal was digitized every 20 μs, and 512 complex points were acquired.

Data analysis. Results from the diffusion measurements are obtained in the form of an echo attenuation *R*, which is defined as the ratio of signal intensities with and without the applied gradient. The plot of signal attenuation *R* as a function of the experimental variable (e.g., δ, Δ, and *g*) can be fit to Equations 2–4 to obtain the size distribution parameters. The FORTRAN computer program ALLFIT, obtained from the Quantum Chemistry Program Exchange at Indiana University (Bloomington, IN), was adapted to find the mean droplet diameter $\bar{a}$ and the standard deviation σ, given in Equation 4, which gave the best fit to our data.

RESULTS AND DISCUSSION

The basic parameters that characterize an emulsion are the emulsion type (i.e., w/o or o/w) and the droplet size distribu-

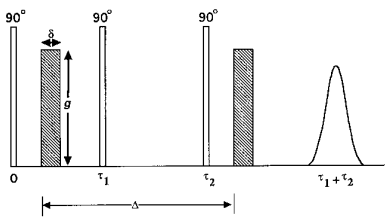

FIG. 1. Pulse sequence of the stimulated echo method.

tion (21). These characteristics are in turn strongly affected by the properties of the emulsifier used to stabilize the system. The properties of emulsions stabilized by two particular emulsifiers, the nonionic surfactant Tween 20 and the milk protein β-Lg, were examined by NMR diffusion methods, with results discussed below.

Emulsion type. The pulse field gradient NMR method can be used to distinguish noninvasively between w/o and o/w types of emulsions, as discussed by Lönnqvist *et al.* (15). In Figure 2, we present the measured signal attenuation R for a Tween 20-stabilized emulsion with 40 wt% octane. In these experiments, we varied the diffusion time Δ from 100 to 1000 ms. To facilitate the determination of the diffusion coefficient of the continuous phase, R is plotted vs. the grouping of experimental parameters $b = (\gamma\ \delta\ g)^2(\Delta - \delta/3)$ (*cf.* Equation 1). Measured signals from the water phase yield a linear dependence of ln(R) on b, indicating that water molecules diffuse unrestrictedly in the system. By applying Equation 1 for unbounded diffusion, the measured diffusivity for water in the emulsion is 2.06×10^{-5} cm^2/s, which differs by less than 2% from the measured value for pure water.

The observed signals from the oil molecules, on the other hand, are almost independent of diffusion time b. This phenomenon suggests that the oil molecules experience restricted diffusion inside droplets. As the diffusion time increases, the extent of diffusional motion of oil molecules is confined by the droplet boundaries, with the result that signal attenuation becomes constant for sufficiently long times. The virtually constant attenuation shown in Figure 2 indicates that the size a of the droplets is small relative to the distance an oil molecule could diffuse freely in the time scale $\sqrt{6D_{oil}\Delta}$, where D_{oil} is the diffusion coefficient of octane. For this experiment and $D_{oil} = 2 \times 10^{-5}$cm^2/s, this observation implies that the droplet radius is much less than 35 μm.

A semiempirical scale, termed the hydrophile–lipophile balance (HLB) by Griffin (22), is often used to predict the type of emulsion formed by a surfactant. Based on the relative percentage of hydrophilic (polar) to hydrophobic (nonpolar) groups in the surfactant molecules, this model indicates that surfactants with a low HLB number (containing more nonpolar groups) normally form w/o emulsions, whereas those with a high HLB number (containing more polar groups) form o/w emulsions. Tween 20 has an HLB number of 16.7, indicating that the surfactant molecules are highly water-soluble and prefer to form o/w emulsions. This prediction is consistent with our results obtained from NMR diffusion measurements. However, if the properties of the surfactant are poorly understood, it can be difficult to predict what type of emulsion will form by using the HLB index. In this situation, NMR diffusion measurements provide a direct and noninvasive method to determine the emulsion type, by monitoring the differences in diffusion behavior between system components.

Droplet sizes upon emulsion formation; effect of emulsifier type. As mentioned above, one of the important roles of emulsifiers during emulsion formation is to lower the interfacial tension between the two phases and thereby reduce the amount of energy needed to break up the droplets. The ability of an emulsifier to accomplish this task depends on its concentration at the o/w interface as that interface is being formed as well as on the energetic interactions of the adsorbed molecules with surrounding phases. Depending on their individual rates of interfacial adsorption as well as their amphiphilicity, different emulsifiers lower the interfacial tension γ to a different extent during emulsion formation, thereby affecting the final size distribution of the emulsion droplets. Here, the emulsifying properties of two major edible emulsifiers, the nonionic surfactant Tween 20 and milk protein β-Lg, are examined.

For an emulsion system, the mean radius $\bar{a}$ and the standard deviation of the droplet sizes can be determined by fitting the experimental data with the restricted diffusion expres-

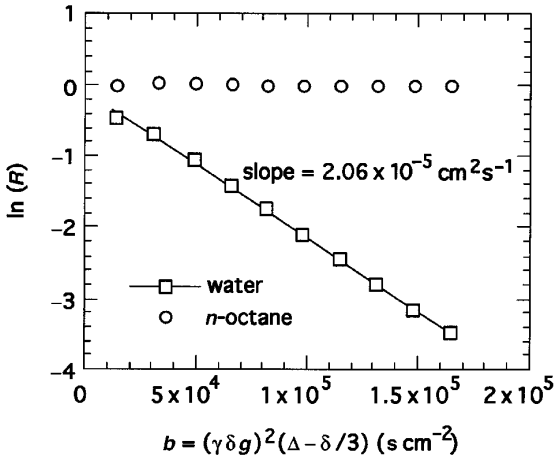

FIG. 2. Natural log of signal attenuation R vs. b, with R determined from signals from both water and oil portions of a 40 wt% octane-in-water emulsion stabilized by 2 wt% Tween 20. δ = 15 ms, g = 1 G/cm.

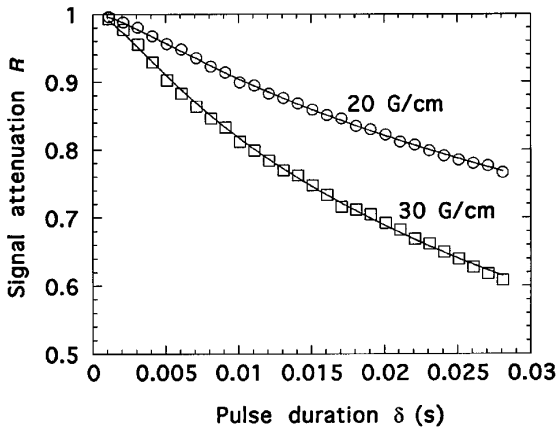

FIG. 3. Signal attenuation vs. pulse duration for a 40 wt% octane-in-D_2O emulsion stabilized by 0.5 wt% Tween 20, measured at two different gradient strengths. Δ = 250 ms.

sion given in Equation 3. In Figure 3, signal attenuation R of an octane-in-D_2O emulsion, stabilized by Tween 20, is plotted as a function of gradient duration δ for two different gradient strength values g of 20 and 30 G/cm. The data were taken with a diffusion time of Δ = 250 ms. By fitting the experimental data with Equation 3, the mean radii $\bar{a}$ and standard deviations obtained from different gradient strengths are virtually identical, with values of $\bar{a} = 1.95 \pm 0.32$ μm and $\bar{a} = 2.03 \pm 0.31$ μm for 20 and 30 G/cm, respectively. The excellent agreement between these results demonstrates the suitability of the monomodal model for the observed signal attenuation.

Figure 4 shows a plot of the measured oil signals as a function of gradient duration δ for emulsions made with 0.1 wt% β-Lg and 0.1 wt% Tween 20, with identical emulsification procedures used for both emulsions. At a gradient strength of g = 3 G/cm, the rapid decay in the attenuation from a protein-stabilized emulsion for values of δ less than 1 ms indicates that the mobility of the oil molecules is not constrained by droplet boundaries over those time scales, implying that the droplets are large in size. For the Tween 20 emulsions, on the other hand, little change in R could be observed at that gradient strength (see dashed line), indicating a much finer emulsion. To expand the sensitivity of our diffusion measurements to these smaller droplets, we increased the gradient strength to 15 G/cm, yielding the results shown in Figure 4. At the higher gradient strength, a significantly attenuated profile for the Tween 20 emulsion can be observed. The results in Figure 4 clearly indicate that the Tween 20 emulsion is much finer than that made with β-Lg.

There are obvious differences between the surface properties of a low-molecular-weight surfactant, such as Tween 20, and the macromolecular β-Lg. In Tween 20, the amphiphilic character of the molecular structure is easily delineated, with three polyoxyethylene groups making up the polar heads and a long hydrocarbon group representing the hydrophobic tail. This simple structure allows the molecule to readily adopt a low-energy conformation at the interface, where its small size and nonionic character lead to high packing densities. The structure of a protein emulsifier is obviously more complicated than that of a low-molecular-weight surfactant and can be less readily described by the idealized head–tail model. Hydrophobic groups, consisting of nonpolar amino acids, are distributed throughout the protein molecule, and their ability to access a nonpolar phase at an interface can require complex rearrangements of the protein's native structure. In β-Lg, the molecule contains one, two or four subunits, each consisting of a single polypeptide chain of 162 amino acids, with a mostly antiparallel β-sheet structure (23,24). Experimental studies show that this globular protein may retain much of its secondary and even part of its tertiary structure after adsorption, to give a thin adsorbed layer of approximately 2 nm in thickness (24).

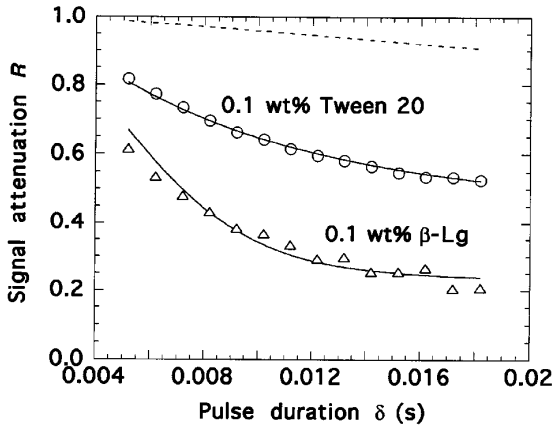

FIG. 4. Signal attenuation vs. pulse duration for a 40 wt% octane-in-D_2O emulsion stabilized by 0.1 wt% β-lactoglobulin (β-Lg) or Tween 20. Gradient strengths used were 3 G/cm for the β-Lg emulsion and 15 G/cm for the Tween 20 emulsion. Δ = 250 ms. To create a stable emulsion with β-Lg, a pH of 9.9 and a Na^+ concentration of 0.1 M were used. Dashed line represents a simulated experimental result from Equation 3 at 3 G/cm, with values for the size distribution parameters obtained from fitting the Tween 20 results at the higher gradient strength.

The clear differences between the two emulsifiers are reflected in their surface activity at a saturated air–water interface: Tween 20 yields an equilibrium surface tension of approximately 36 dynes/cm (25), compared to 55 to 60 dynes/cm for β-Lg (26). The ability of β-Lg to lower the oil–water tension during emulsification is thus likely to be weaker than that of Tween 20 (4,27). The difference in adsorption kinetics between the two surfactants is also important. Because surfactant adsorption rates are often slow relative to the rate of droplet formation, there may not be sufficient time for the emulsifier to saturate and lower the tension of the newly formed interface. The much larger diffusion coefficient for β-Lg compared to Tween 20 indicates that such adsorption limitations will be more severe for the protein emulsifier, thus further decreasing the effectiveness of β-Lg in forming emulsions compared to low-molecular-weight surfactants (28).

Droplet sizes upon emulsion formation; effect of emulsifier concentration. In addition to the nature of the emulsifier, emulsion droplet size is directly affected by emulsifier concentration because this concentration determines the surface excess of surfactant, and hence the degree to which the interfacial tension is lowered. For this reason, octane-in-D_2O emulsions with three different concentrations of Tween 20, ranging from 0.1 to 3.0 wt%, were prepared in the same fashion and examined by the NMR diffusion technique. The oil signals from emulsions stabilized by 0.1, 0.5, 1.5, and 3.0 wt% Tween 20 are plotted as a function of δ in Figure 5. Clearly, for concentrations above 0.5 wt%, the attenuation profiles show no dependence of diffusion behavior on surfactant concentration, suggesting that the emulsion droplet sizes are approximately the same in all these samples. For the lowest concentration of Tween 20, significantly larger drops appear to be formed, as shown by the more rapid attenuation decay, even at a lower gradient strength (see dotted line for

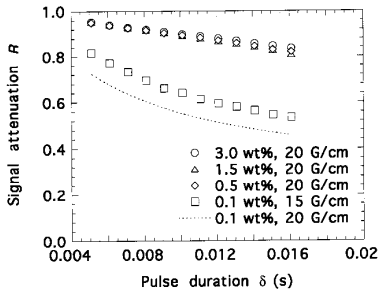

FIG. 5. Signal attenuation vs. pulse duration for a 40 wt% octane-in-D_2O emulsion stabilized by Tween 20. Gradient strength was 15 G/cm for the 0.1 wt% Tween 20 emulsion, and 20 G/cm for all other concentrations. Δ = 250 ms. Dashed line represents a simulated experimental result from Equation 3 at 20 G/cm, with values for the size distribution parameters obtained from fitting the 0.1 wt% result at 15 G/cm.

direct comparison).

By using Equation 3 to fit the data in Figure 5, we find that the emulsions formed with Tween 20 concentrations between 0.5 and 3.0 wt% are fairly monodisperse, with a mean diameter of approximately 3.4–3.7 μm. Using these values and the density $\rho = 7.0 \times 10^5$ g/m^3 of *n*-octane, we estimate the specific area in these emulsions to be approximately 1 m^2 per gram of emulsion. Given the literature value for the excess surface concentration $\Gamma = 2.8 \times 10^{-3}$ g/m^2 for an interface saturated with Tween 20 (29), we then determine that the amount of surfactant needed to cover fully the oil droplet surfaces in these emulsions is about 3×10^{-3} g per gram of emulsion, or 0.47 wt% surfactant in the aqueous phase. Thus, the emulsions formed from surfactant concentrations between 0.5 and 1.5 wt% appear to have more than enough surfactant to saturate the interfacial area formed. For surfactant concentrations above 0.5 wt%, the drop sizes are no longer constrained by the surfactant available to coat them. Instead, the minimal drop size is determined by the limiting interfacial tension achieved at interfacial saturation, coupled with the energy input by the homogenizer.

Comparison of the data in Figure 5 with Equation 3 indicates that a bimodal dispersion is formed when 0.1 wt% Tween 20 is used, in contrast to the emulsions discussed above. Approximately half of the oil volume is contained in droplets of mean diameter 1.8 μm, while the other half of the oil forms larger droplets, with mean diameter 4.6 μm. This more complex distribution appears to result from insufficient Tween 20 to form the uniform drops found at the other concentrations. With 0.1 wt% Tween 20 emulsions, the smaller population of droplets contributes approximately 1 m^2 per gram of emulsion—a value similar to that found in the emulsions with higher surfactant concentrations. Much of the surfactant in solution may go to forming these smaller droplets, leaving little surfactant for the remainder of the oil, and hence resulting in a significantly larger second population of drops. However, 0.1 wt% Tween 20 in the aqueous phase is insufficient to saturate even the population of small drops, suggesting either that interfacial saturation is not necessary for droplet formation, or that the fit of Equation 3 underestimates the droplet sizes.

Droplet sizes upon emulsion formation; effect of pH. In response to any changes in environmental conditions, e.g., pH and temperature, proteins may undergo conformational rearrangement to minimize the molecular free energy. In addition, such conditions can influence the way proteins interact with each other at the interface. Such conformational changes and protein/protein interactions can directly affect the surface activity and functionality of protein molecules at the interface.

In Figure 6, the restricted diffusion measurement of an emulsion stabilized by β-Lg is plotted for different pH values. As pH increases, enhanced diffusional freedom of the oil molecules inside the droplets is observed, indicating that emulsification forms larger droplets as pH goes up. This result implies that the emulsifying properties of β-Lg decrease with increasing pH. This phenomenon is in contrast with the observations of Das and Kinsella (30) and Relkin *et al.* (31) who reported that the emulsifying properties of β-Lg are improved at higher pH, so that finer emulsion droplets were formed. The discrepancy between these results may be attributed to different particle characterization methods. The NMR–PFG technique measures the dimension of the drops by monitoring the molecular diffusion inside the individual droplets, whereas the turbidity

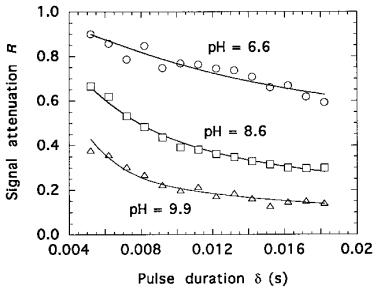

FIG. 6. Signal attenuation vs. pulse duration for a 40 wt% octane-in-D_2O emulsion stabilized by β-Lg. Salt concentration is 0.1 M. Gradient strength was 5 G/cm and Δ = 250 ms. Solid curves are fits of Equation 3 to the data. See Figure 4 for abbreviation.

measurements used by Das and Kinsella (30) and Relkin *et al.* (31) determine the intensity of scattered light from a collection of emulsion particles. For protein-stabilized emulsions, two or more droplets may cluster together to form an aggregate when the electrostatic repulsion between them is at a minimum, in particular at pH values around the isoelectric point (pI), where the protein molecule is effectively neutral. In addition, flocculation due to macromolecular bridging can also be promoted at pH values near the pI. Once flocculation occurs, turbidity measurements may not distinguish such flocs from large single droplets. Therefore, the reported increase in droplet size around the pI detected by Das and Kinsella (30) and Relkin *et al.* (31) may be caused by multiple scattering from flocculated droplets, rather than by reducing the effectiveness of emulsification.

Because β-Lg, like all proteins, is a polyelectrolyte, the pH of the surrounding solution greatly affects the net surface charge and the charge distribution on the molecule. Because most of the charged amino acids reside at the exterior of protein molecules, the surface charge of proteins often determines the surface activity of the molecules (32). Experimental evidence shows that the rate of adsorption to an interface and resulting surface pressure of β-Lg are markedly pH-dependent, showing a sharp maximum near the pI (33). The optimal adsorption of β-Lg around the pI is mainly attributed to the minimal electrostatic repulsion among adsorbed molecules, so that β-Lg can adopt the most compact configuration and pack easily at the interface (34). At higher pH values, literature data clearly indicate that the electrostatic interaction between charged residues causes not only the conformational changes in the protein but also an expansion in "effective" size of β-Lg (35). Such an increase in molecular size requires more cleared area of the interface for the penetration of newly adsorbed protein molecules (33) and thus causes a lower surface coverage of β-Lg at higher pH. This lower surface coverage should in turn mean higher interfacial tensions and reduced emulsifying capabilities.

In addition to structural changes, the surface charge on a protein may create two types of electrostatic potential barriers to adsorption at the interface. In the initial stage of adsorption, when the surface is "clean" and free of charged molecules, the protein molecule experiences a repulsive potential $U_0 = (q_p{}^2/2d\varepsilon_a)(\varepsilon_a - \varepsilon_o)/(\varepsilon_a + \varepsilon_o)$ at a distance d from the interface (36), where q_p is the net charge on the protein and ε_a and ε_o are the dielectric constants of the aqueous and the oil phase, respectively. As the adsorption process continues, the adsorbed protein molecules create an additional electrostatic barrier U_1 at the interface, given by $U_1 = \int_0^{qi} \psi_i \, dq$, where q_i is the charge at the interface due to the adsorbed protein. Here, ψ_i is the electrical potential per unit charge at the interface, created by the interaction between the double layers of the protein molecule and the interface (37). This potential is proportional to the charge on the protein q_p, the interfacial charge q, which itself depends linearly on q_p, and the double layer thickness. For β-Lg, Cannan *et al.* (38) report that the net surface charge q_p is approximately −11.5 at pH 6.6, and progressively increases to −30 at pH 9.9. The almost threefold increase in surface charge at pH 9.9 would have a ninefold effect on U_0 and U_1, creating a substantially higher potential barrier for β-Lg to approach the charged interface. Such an increase in pH should hence have the effect of decreasing the adsorption rate and surface pressure as compared to values obtained at pH 6.6.

Droplet sizes upon emulsion formation; effect of salt concentration. If electrostatic interactions do indeed alter the surface activity of β-Lg as the pH is increased, one might expect some influence of ionic strength on emulsion properties. In particular, the potential barrier to adsorption depends on the double layer thickness, which decreases as the ionic strength increases. Therefore, the effect of electrostatic forces at the interface is expected to be diminished at higher salt concentrations, owing to the screening effect of the neighboring ions. This trend is indeed manifested in our restricted diffusion measurements. When we add sufficient NaCl to increase the cation concentration from 0.1 M to 1.0 M, we again observe larger droplet sizes in emulsion samples with increased pH values, as shown in Figure 7. However, the difference between samples is clearly reduced at the higher salt concentration, thus affirming the importance of electrostatic interactions on the emulsifying properties of β-Lg.

We can further investigate the effect of ionic strength on the effectiveness of the protein in the emulsification process by plotting results for various electrolyte concentrations at a fixed pH value. The restricted diffusion behavior of an octane-in-D_2O emulsion, stabilized by β-Lg at pH 9.9, is shown in Figure 8. In these experiments, the concentration of NaCl was increased from 0.1 M to 1.0 M, and the results indicate that the domain available for oil diffusion increases with in-

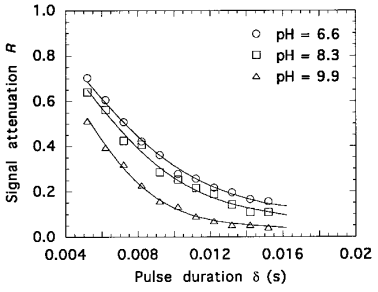

FIG. 7. Signal attenuation vs. pulse duration for a 40 wt% octane-in-D_2O emulsion stabilized by β-Lg. Salt concentration is 1 M. Gradient strength was 3 G/cm and Δ = 250 ms. Solid curves are fits of Equation 3 to the data. See Figure 4 for abbreviation.

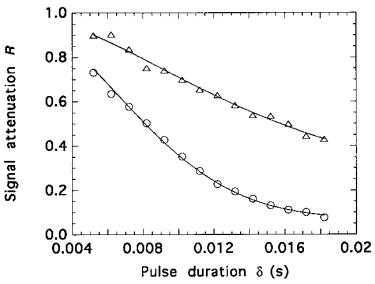

FIG. 8. Signal attenuation vs. pulse duration for a 40 wt% octane-in-D_2O emulsion stabilized by β-Lg. pH is 9.9, and NaCl concentrations are 1 M (○) and 0.1 M (Δ). Gradient strength was 2 G/cm and Δ = 250 ms. Solid curves are fits of Equation 3 to the data. See Figure 4 for abbreviation.

creasing salt, as shown by the stronger dependence of the signal attenuation on δ. Thus, the mean droplet diameter increases with increasing NaCl concentration. This observation agrees well with results reported by Agboola and Dalgleish (39) and Mita *et al.* (40). However, this trend is opposite to what we would expect if electrostatic interactions are primarily important in determining the emulsifying properties of β-Lg. Because the addition of NaCl in the solution "shields" the charges on the protein molecule (by decreasing the double layer thickness), reduction of electrostatic repulsion between β-Lg molecules is anticipated at high ionic strengths, with this effect particularly pronounced at pH 9.9. As already explained, such a reduction should lead to higher surface concentrations of protein and therefore enhance the emulsifying ability of β-Lg as salt concentration increases. The fact that such an enhancement is not observed in the results in Figure 8 suggests that, in addition to electrostatic forces, other factors may also play a role in the adsorption behavior of β-Lg at the oil/water interface.

Reports in the literature indicate that the effect of NaCl on the surface activity of β-Lg is complex. At low ionic strengths, the surface tension of dilute aqueous β-Lg solutions has been shown to decrease with increasing salt concentration (36). This result implies that higher surface adsorption results at higher salt concentrations. On the other hand, at high values of ionic strength and more concentrated protein solutions, Luey *et al.* (35) found that the adsorption of β-Lg on a hydrophobic silicon surface decreased as NaCl concentration increased from 0.1 to 0.5 M. Tornberg (41) also reported that the adsorption of whey protein concentrate, which contains more than 50% β-Lg, on a soy oil/water interface was reduced when 0.2 M NaCl was added to the system. These studies at high ionic strengths indicate that the surface activity of β-Lg is diminished in the presence of NaCl, consistent with our observations of its effect on emulsifying activity. It is possible that, at high ionic strengths, electrostatic interactions between proteins in solution are reduced, while the added interactions between salt and water enhance protein hydrophobicity. Such a "salting out" effect could lead to the formation of large protein aggregates in solution or even to precipitation (35,42). Large or insoluble proteins would not be active at the interface (31), and thus the emulsifying properties of β-Lg would be adversely affected.

Coalescence stability of emulsion droplets. Because emulsions are thermodynamically unstable, given sufficient time, droplets will coalesce to form larger ones and cause eventual phase separation. By monitoring the extent of molecular diffusion within droplets as a function of time, we extended our NMR diffusion measurements to detect increases in droplet sizes due to coalescence.

Coalescence stability of emulsion droplets; effect of convection. Coalescence between droplets requires three steps: (i) an encounter between droplets (flocculation); (ii) drainage of the thin liquid film between two droplets; and (iii) film rupture caused by surface instabilities. Coalescence kinetics can be dominated by the mechanism associated with one or more of these steps, depending on their relative rates. To explore the importance of flocculation kinetics in the overall droplet coalescence mechanism, we studied the effect of convective motion on emulsion stability.

Convection in our sample was mechanically induced by rotating the sample end-on-end vertically at a speed of six revolutions per minute. Figure 9 shows a plot of oil signals as a function of gradient duration δ for spun samples of a 0.1 wt% Tween 20 emulsion. These profiles of the signal attenuation were taken at 1-d intervals over the 3 d of the experiment, with the emulsions spun continuously throughout. Figure 9 indicates

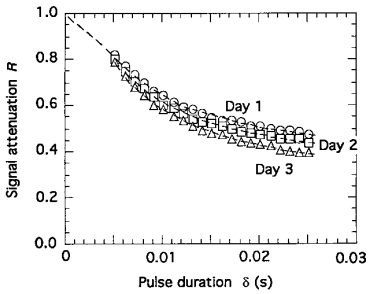

FIG. 9. Signal attenuation vs. pulse duration for a 40 wt% octane-in-D_2O emulsion stabilized by 0.1 wt% Tween 20. Signal taken after emulsion was left quiescent for 1, 2, and 3 d. Gradient strength was 15 G/cm and Δ = 250 ms. Curves are fits of Equation 3 to the data.

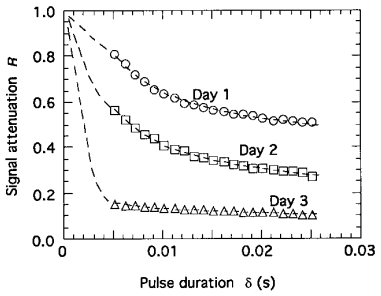

FIG. 10. Signal attenuation vs. pulse duration for a 40 wt% octane-in-D_2O emulsion stabilized by 0.1 wt% Tween 20. Signal taken after emulsion was spun at 6 rpm for 1, 2, and 3 d. Gradient strength was 15 G/cm and Δ = 250 ms. Curves are fits of Equation 3 to the data.

an increasingly rapid decay in the attenuation of the oil signals over time, which suggests an associated increase in diffusion domain within the droplets. Conversely, in the absence of convection, Figure 10 shows apparently little change in diffusion domain for an identical but quiescent emulsion over 3 d. This result implies that the unspun emulsion was relatively stable to coalescence during the measurement period.

Values for the mean droplet diameter $\bar{d}$ were obtained by fitting Equation 3 to the data in Figures 9 and 10, assuming a monomodal distribution for the droplet diameters. Here, the diameter is twice the radius ($\bar{d} = 2\bar{a}$). These values and their standard deviations σ are given in Table 1. For the quiescent emulsion, the simple monomodal distribution fitted the data well, yielding a mean diameter of 2.6 to 2.8 μm as shown in the table. The values for the mean droplet diameter and standard deviation increased only slightly over the 3 d of the experiment, supporting our qualitative observation from Figure 10 that little or no coalescence occurred during this time. As for the spun emulsion, the induced convection led to a change in the qualitative shape of the size distribution because we were unable to fit the measured attenuation at days 2 and 3 by using a simple monomodal distribution. Instead, a bimodal distribution was used to quantify the changes observed in this sample.

TABLE 1
Comparison of Droplet Sizes in Quiescent and Spun Emulsions, Assuming a Monomodal Distribution[a]

	Quiescent emulsion		Spun emulsion	
	$\bar{d}$ (μm)	σ	$\bar{d}$ (μm)	σ
Day 1	2.6	0.65	1.4	0.78
Day 2	2.8	0.65	—	—
Day 3	3.8	0.58	—	—

[a]Emulsions contained 0.1 wt% Tween 20 in an octane-in-D_2O emulsion.

Table 2 compares the mean diameters for two populations ("small" and "large") of droplets within the spun emulsion, as well as the number fraction ϕ of each population. To reduce the number of fit parameters, we assumed that the shape of the populations stayed constant throughout the experiment, and thus fixed σ_{small} and σ_{large} to the values obtained from the emulsion on day 1. We note that, although the number fraction of large droplets is quite small, their volume is considerable, and they have a significant effect on the observed attenuation (as indicated by the fact that the attenuation must be modeled with a bimodal distribution). Also shown in Table 2, for purposes of comparison, are the results obtained from fitting a bimodal distribution to data from the quiescent emulsion. The resulting values for the mean diameter show little change over time, consistent with results shown in Table 1.

The spun emulsions, on the other hand, show a clear increase in droplet size over the 3 d of the experiment. For the small droplets, the mean diameter more than doubles in size, whereas the influence on the large population is even greater, with almost an order of magnitude increase. There also appears to be a shift in volume from small droplets to large. The results of this experiment seem to indicate that coalescence is more rapid between larger droplets than smaller. To verify qualitatively the conclusions extracted from Table 2, we also examined samples of the spun emulsion over the 3 d of the experiment under a Leitz Dialus 20 microscope. Images from these micrographs are given in Figures 11A and 11B and show a clear increase in droplet size over time. Figure 11 thus provides direct visual evidence of the destabilizing effect of coalescence.

The results presented in Figures 9 through 11 and in Tables 1 and 2 demonstrate a significant effect of convection on the rate of coalescence in these concentrated emulsions. For coalescence to occur, droplets must first encounter each other in a flocculation step and then must merge through film-thinning and film-rupture processes. The presence of convection is expected primarily to enhance the first of these steps, by augmenting the frequency of encounters between particles. Hence, the results discussed above point to flocculation as the rate-limiting step in the coalescence of these droplets. At a 0.1 wt% concentration of Tween 20, the purely steric barriers to film thinning and rupture presented by this nonionic surfactant appear to be low enough that these later steps in coalescence are rapid compared to flocculation.

A useful feature of these NMR self-diffusion measurements is that increases in droplet sizes are only detected if the droplets actually coalesce. Clustering of droplets due to flocculation does not affect signal attenuation unless the droplets actually experience film-thinning and rupture. This feature distinguishes NMR from other approaches, such as light-scattering or Coulter principle measurements. This aspect of the NMR droplet-sizing technique is a consequence of the fact that the domain sampled by oil molecules within the droplet is what is actually monitored. Thus, our measurements provide key information needed to determine the relative impor-

TABLE 2
Comparison of Droplet Sizes in Quiescent and Spun Emulsions, Assuming a Bimodal Distribution[a]

	Quiescent emulsion ($\sigma_{small} = 0.33$; $\sigma_{large} = 0.53$)[b]			Spun emulsion ($\sigma_{small} = 0.32$; $\sigma_{large} = 0.57$)[b]		
	$\bar{d}_{small}$ (μm)	$\bar{d}_{large}$ (μm)	ϕ_{small}	$\bar{d}_{small}$ (μm)	$\bar{d}_{large}$ (μm)	ϕ_{small}
Day 1	1.6	4.9	0.936	1.8	4.6	0.953
Day 2	1.4	4.8	0.949	5.8	10	0.914
Day 3	1.4	5.0	0.906	5.3	42	0.995

[a]Emulsions contained 0.1 wt% Tween 20 in an octane-in-D_2O emulsion.
[b]Standard deviations for each population were obtained from fits to the data at day 1, then held constant in fits to days 2 and 3.

tance of flocculation and coalescence steps in the overall destabilization process.

A less desirable aspect of using NMR diffusion measurements to determine droplet sizes is that we must assume a model for the size distribution to quantify the data. The more complex the assumed distribution, the more parameters we must fit to capture the measured signal, thus increasing the uncertainty associated with any one parameter. NMR methods are similar in this respect to most standard light-scattering approaches, where again a model for the droplet size distribution is assumed. With the NMR technique, this disadvantage can be minimized to some extent by varying experimental parameters, such as gradient strength (*cf.* Fig. 3) or diffusion time Δ between gradient pulses. These alterations have the effect of "weighting" different portions of the droplet population as the measurement technique becomes more or less sensitive to droplets in a particular size range. Microscopy avoids these difficulties by direct inspection of the emulsion; however, microscopic visualization is significantly more invasive and laborious than NMR techniques and examines only small portions of the emulsion at a time.

Coalescence stability of emulsion droplets; effect of surfactant concentration. The results presented in Figures 9 and 10 can be compared with signal attenuation in emulsions with higher surfactant concentrations of 0.3 and 0.5 wt% Tween 20. This comparison allows us to investigate the effect of surfactant concentration on overall interfacial stability. The amount of hydrocarbon in each emulsion is again set to 40 wt% of the total sample. Results obtained from these samples at a gradient strength of 15 G/cm and a diffusion time Δ = 250 ms are shown in Figures 12 and 13 as a function of gradient duration δ. Even in the presence of convection (spinning), both samples show little change in their attenuation profiles during the course of the experiments, in contrast to the emulsion stabilized by 0.1 wt% Tween 20. These results are quali-

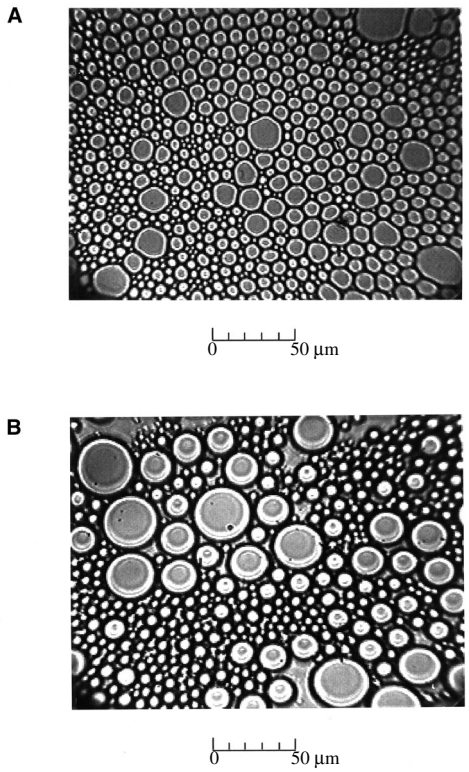

FIG. 11. Micrograph of a 40 wt% octane-in-D_2O emulsion stabilized by 0.1 wt% Tween 20. Image taken after emulsion was spun (A) 1 d and (B) 3 d.

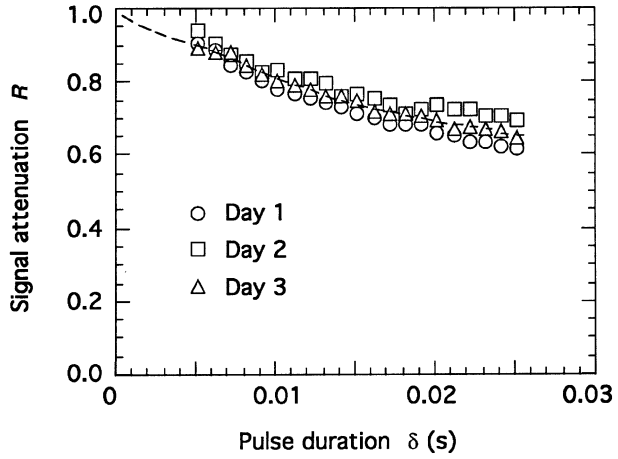

FIG. 12. Signal attenuation vs. pulse duration for a 40 wt% octane-in-D_2O emulsion stabilized by 0.3 wt% Tween 20. Signal taken after emulsion was spun at 6 rpm for 1, 2, and 3 d. Gradient strength was 15 G/cm and Δ = 250 ms. Curve is fit of Equation 3 to the data.

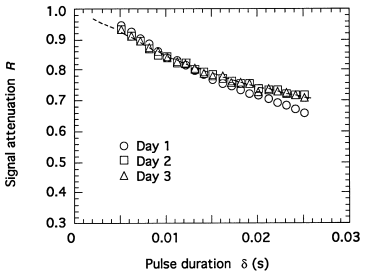

FIG. 13. Signal attenuation vs. pulse duration for a 40 wt% octane-in-D_2O emulsion stabilized by 0.5 wt% Tween 20. Signal taken after emulsion was spun at 6 rpm for 1, 2, and 3 d. Gradient strength was 15 G/cm and $\Delta = 250$ ms. Curve is fit of Equation 3 to the data.

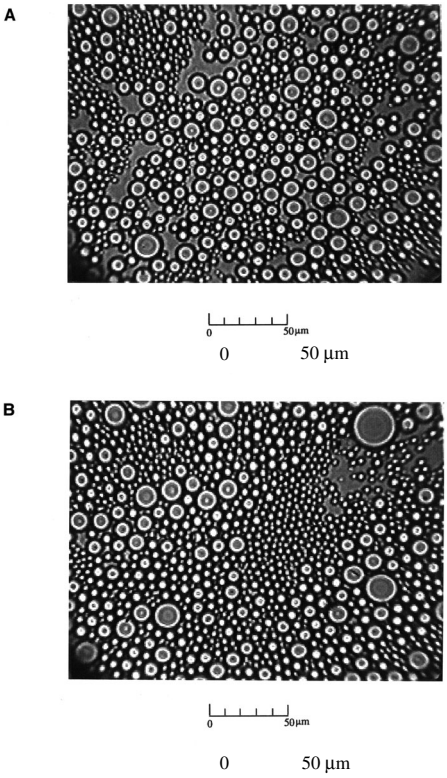

FIG. 14. Micrograph of a 40 wt% octane-in-D_2O emulsion stabilized by 0.5 wt% Tween 20. Image taken after emulsion was spun (A) 1 d and (B) 3 d.

tatively verified by direct micrographic examination. As shown in Figure 14 for 0.5 wt% Tween 20, no observable changes in the droplet sizes occurred over the 3 d of the experiment.

These results indicate that an increase in Tween 20 concentration enhances emulsion stability to coalescence. The three concentrations examined here—0.1, 0.3, and 0.5 wt%—are expected to be substantially below, somewhat below, and slightly above the concentration required for a saturated interface (see discussion above). At a saturated interface, Tween 20 molecules have achieved their maximal packing, creating a high-potential barrier between droplets through steric interactions. In addition, such a closely packed interface means that drainage of liquid between drops will be resisted by strong tangential stresses within the interface. The fact that coalescence kinetics become independent of the presence or absence of convection at these higher surfactant concentrations suggests that film thinning and/or rupture has become sufficiently slow that flocculation kinetics are no longer rate-limiting. However, it is also possible that the stronger steric barrier presented by the surfactant headgroups has slowed down collision rates sufficiently that they are no longer detectable over the 3 d of the experiment.

Coalescence stability of emulsion droplets; effect of surfactant type. The stability of emulsions formed with Tween 20 can be compared with similar measurements on emulsions formed from the milk protein β-Lg. Figure 15 shows the signal attenuation of a 40 wt% emulsion at a pH of 9.0 and a salt concentration of 2.0 M. Although these experiments were conducted in the absence of convection, the measurements were taken over a 2-wk period. The results in Figure 15 show no difference in signal attenuation over 14 d, indicating that no coalescence occurred in these emulsions over that time period. Emulsions prepared at lower salt concentrations (down to 0.1 M) were similarly stable to coalescence.

The stability of these protein-stabilized emulsions is particularly interesting in light of the difference in emulsion-forming capabilities of β-Lg and Tween 20. As shown in Figures 4 and 6, at high pH values, β-Lg forms much larger droplets than does Tween 20, owing to the less effective adsorption of the large charged protein to the interface. However, once present, the adsorbed protein film apparently provides at least as effective a barrier to coalescence as Tween 20. At high pH, the protein is highly charged, creating electrostatic repulsion between droplets. However, the stability of these emulsions to high salt concentrations indicates that non-electrostatic phenomena also play important roles: steric interactions between bulky protein molecules and the ability of the adsorbed protein film to withstand tangential interfacial stresses retard film thinning and film rupture (41). In fact, Boyd *et al.* (43) reported that β-Lg forms viscous surface films with good mechanical properties, in contrast to disordered and flexible proteins, such as caseins.

As the pH is lowered to the pI, however, we do see clear indications of emulsion destabilization. These emulsions show visible effects of creaming within minutes after preparation. As discussed above, the emulsions prepared at this pH initially contain smaller droplets than those formed at a pH of

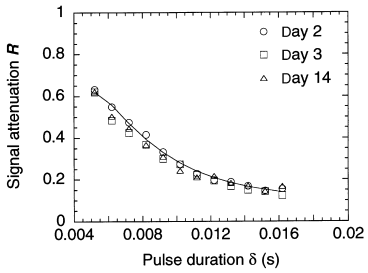

FIG. 15. Signal attenuation vs. pulse duration for a 40 wt% octane-in-D_2O emulsion stabilized by 0.1 wt% β-Lg at pH = 9.0 and a salt concentration of 2 M. Signal taken after emulsion was left quiescent for 2, 3, and 14 d. Gradient strength was 3 G/cm and Δ = 250 ms. Curve is fit of Equation 3 to the data. See Figure 4 for abbreviation.

9.0, and thus the difference in creaming rates in these two emulsions must be attributed to rapid flocculation of droplets at a pH near the pI. Reduction of charge at these pH values apparently allows the droplets to cluster rapidly to form larger aggregates, which rise quickly to the top of the sample.

ACKNOWLEDGMENTS

We gratefully acknowledge Kraft Foods for supporting this research. This work was also partially supported by an NSF Young Investigator Award CTS-93-58508 to SRD. The authors express their sincere thanks to Professor David Reid for the use of his microscope.

REFERENCES

1. Lobo, L.A., and D.T. Wasan, Thin Film Stability and Interfacial Rheology of Emulsion Systems, in *Food Emulsion and Foams: Theory and Practice*, edited by P.J. Wan, J.L. Cavallo, F.Z. Saleeb, and M.J. McCarthy, American Institute of Chemical Engineers, New York, 1990, pp. 25–34.
2. Chen, J., E. Dickinson, and G. Iveson, Interfacial Interactions, Competitive Adsorption and Emulsion Stability, *Food Structure 12*:135–146 (1993).
3. Hassander, H., B. Johansson, and B. Tornell, The Mechanism of Emulsion Stabilization by Small Silica (Ludox) Particles, *Colloids Surf. 40*:93–105 (1989).
4. Das, K.P., and J.E. Kinsella, Droplet Size and Coalescence Stability of Whey Protein Stabilized Milkfat Peanut Oil Emulsions, *J. Food Sci. 58*:439–444 (1993).
5. Tornberg, E., and N. Ediriweera, Coalescence Stability of Protein-Stabilized Emulsions, in *Food Emulsions and Foams*, edited by E. Dickinson, The Royal Society of Chemistry, London, 1987, pp. 52–63.
6. Melsen, J.P., and P. Walstra, Stability of Recombined Milk-Fat Globules, *Neth. Milk Dairy J. 43*:63–78 (1989).
7. Klemaszewski, J.L., K.P. Das, and J.E. Kinsella, Formation and Coalescence Stability of Emulsions Stabilized by Different Milk Proteins, *J. Food Sci. 57*:366–371,379 (1992).
8. Dickinson, E., and A. Williams, Orthokinetic Coalescence of Protein-Stabilized Emulsions, *Colloids Surf. A: Physicochem. Eng. Aspects 88*:317–326 (1994).
9. Britten, M., and H.J. Giroux, Coalescence Index of Protein-Stabilized Emulsions, *J. Food Sci. 56*:792–795 (1991).
10. Haque, Z., and J.E. Kinsella, Relative Emulsifying Activity of Bovine Serum Albumin and Casein as Assessed by Three Different Methods, *Ibid. 54*:1341–1344 (1989).
11. Packer, K.J., and C. Rees, Pulsed NMR Studies of Restricted Diffusion. I. Droplet Size Distributions in Emulsions, *J. Colloid Interface Sci. 40*:206–218 (1972).
12. Callaghan, P.T., J.W. Jolley, and R.S. Humphrey, Diffusion of Fat and Water in Cheese as Studied by Pulsed Field Gradient Nuclear Magnetic Resonance, *Ibid. 93*:521–529 (1983).
13. Van den Enden, J.C., D. Waddington, H. Van Aalst, C.G. Van Kralingen, and J.K. Packer, Rapid Determination of Water Droplet Size Distributions by PFG–NMR, *Ibid. 140*:105–113 (1990).
14. Li, X., J.C. Cox, and R.W. Flumerfelt, Determination of Emulsion Size Distribution by NMR Restricted Diffusion Measurement, *AIChE J. 38*:1671–1674 (1992).
15. Lönnqvist, I., A. Khan, and O. Söderman, Characterization of Emulsions by NMR Methods, *J. Colloid Interface Sci. 144*:401–411 (1991).
16. Abragam, A., *The Principles of Nuclear Magnetism*, Clarendon Press, Oxford, 1961, pp. 19–22.
17. Stejskal, E.O., and J.E. Tanner, Spin Diffusion Measurements: Spin Echoes in the Presence of a Time-Dependent Field Gradient, *J. Chem. Phys. 42*:288–292 (1965).
18. Murday, J.S., and R.M. Cotts, Self-Diffusion Coefficient of Liquid Lithium, *J. Chem. Phys. 48*:4938–4945 (1968).
19. Hahn, E.L., Spin Echoes, *Phys. Rev. 80*:580–594 (1950).
20. Callaghan, P.T., *Principles of Nuclear Magnetic Resonance Microscopy*, Clarendon Press, Oxford, 1991, pp. 157–166.
21. Walstra, P., Principles of Emulsion Formation, *Chem. Eng. Sci. 48*:333–349 (1993).
22. Griffin, W.C., Classification of Surface-Active Agents by "HLB," *J. Soc. Cosm. Chem. 1*:311–326 (1949).
23. Jaynes, E.N., Applications in the Food Industry: II, in *Encyclopedia of Emulsion Technology*, Vol. 2, edited by P. Becher, Marcel Dekker, New York, 1985, pp. 367–384.
24. Dalgleish, D.G., and J. Leaver, The Possible Conformations of Milk Proteins Adsorbed on Oil Water Interfaces, *J. Colloid Interface Sci. 41*:288–294 (1991).
25. Schönfeldt, N., *Surface Active Ethylene Oxide Adducts*, Pergamon Press, Oxford, 1969, p. 169.
26. Suttiprasit, P., V. Krisdhasima, and J. McGuire, The Surface Activity of α-Lactalbumin, β-Lactoglobulin, and Bovine Serum Albumin. 1. Surface Tension Measurements with Single-Component and Mixed Solutions, *J. Colloid Interface Sci. 154*:316–326 (1992).
27. Dickinson, E., Adsorbed Protein Layers in Food Emulsions, in *Emulsions—A Fundamental and Practical Approach*, edited by J. Sjöblom, Kluwer Academic, Dordrecht, 1992, pp. 25–40.
28. Velev, O.D., T.D. Gurkov, S.K. Chakarova, B.I. Dimitrova, I.B. Ivanov, and R.P. Borwankar, Experimental Investigations on Model Emulsion Systems Stabilized with Non-Ionic Surfactant Blends, *Colloids Surf. A: Physicochem. Eng. Aspects 83*:43–55 (1994).
29. Wan, L.S.C., and P.F.S. Lee, Influence of Nonionic Surfactants on Interfacial Tension in an Oil–Water System, *Can. J. Pharm. Sci. 8*:136–139 (1973).
30. Das, K.P., and J.E. Kinsella, pH Dependent Emulsifying Properties of β-Lactoglobulin, *J. Dispersion Sci. Technol. 10*:77–102 (1989).
31. Relkin, P., R. Liu, and B. Launay, Effects of pH on Gelation and

Emulsification of a β-Lactoglobulin Concentrate, *Ibid. 14*:335–354 (1993).
32. Horbett, T.A., and F.L. Brash, Proteins at Interfaces: Current Issues and Future Prospects, in *Proteins at Interfaces: Physicochemical and Biochemical Studies*, edited by F.L. Brash and T.A. Horbett, American Chemical Society, Washington, D.C., 1987, pp. 1–35.
33. Waniska, R.D., and J.E. Kinsella, Surface Properties of β-Lactoglobulin: Adsorption and Rearrangement During Film Formation, *J. Agric. Food Chem. 33*:1143–1148 (1985).
34. Kinsella, J.E., and D.M. Whitehead, Film, Foaming, and Emulsifying Properties of Food Proteins: Effects of Modification, in *Proteins at Interfaces: Physicochemical and Biochemical Studies*, edited by F.L. Brash and T.A. Horbett, American Chemical Society, Washington, D.C., 1987, pp. 629–646.
35. Luey, J., J. McGuire, and R.D. Sproull, The Effect of pH and NaCl Concentration on Adsorption of β-Lactoglobulin at Hydrophilic and Hydrophobic Silicon Surfaces, *J. Colloid Interface Sci. 143*:489–500 (1991).
36. Song, K.B., and S. Damodaran, Influence of Electrostatic Forces on the Adsorption of Succinylated β-Lactoglobulin at the Air–Water Interface, *Langmuir 7*:2737–2742 (1991).
37. Hunter, R.J., *Foundations of Colloid Science,* Clarendon Press, Oxford, 1986, pp. 415–418.
38. Cannan, R.K., A.H. Palmer, and A.C. Kibrick, Hydrogen-Ion Dissociation Curve of β-Lactoglobulin, *J. Biol. Chem. 142*:803–822 (1942).
39. Agboola, S.O., and D.G. Dalgleish, Calcium-Induced Destabilization of Oil-in-Water Emulsions Stabilized by Caseinate or by β-Lactoglobulin, *J. Food Sci. 60*:399–404 (1995).
40. Mita, T., E. Iguchi, K. Yamada, S. Matsumoto, and D. Yonezawa, Dispersion State of Protein-Stabilized Emulsions. II. Effect of Sodium Chloride on Stability of Oil-in-Water Systems, *J. Texture Stud. 5*:89–96 (1974).
41. Tornberg, E., Functional Characterisation of Protein Stabilised Emulsions: Emulsifying Behaviour of Proteins in a Valve Homogeniser, *J. Sci. Food Agric. 9*:867–879 (1978).
42. Arakawa, T., and S.N. Timasheff, Abnormal Solubility Behavior of β-Lactoglobulin: Salting-In by Glycine and NaCl, *Biochemistry 6*:5147–5153 (1987).
43. Boyd, J.V., J.R. Mitchell, L. Irons, P.R. Musselwhite, and P. Sherman, The Mechanical Properties of Milk Protein Films Spread at the Air-Water Interface, *J. Colloid Interface Sci. 45*:478–486 (1973).

[Received September 23, 1996; accepted September 2, 1997]